Probability Distribution of Turbulent Kinetic Energy Dissipation Rate in Ocean: Observations and Approximations

6 authors, including:

Iossif Lozovatsky
University of Notre Dame
72 PUBLICATIONS   1,040 CITATIONS

SEE PROFILE

Zhiyu Liu
Xiamen University
61 PUBLICATIONS   1,212 CITATIONS

SEE PROFILE

Jae Hak Lee
Korean Institute of Ocean Science and Technology
67 PUBLICATIONS   1,367 CITATIONS

SEE PROFILE

Sinhalage Jinadasa
National Aquatic Resources Research and Development Agency
55 PUBLICATIONS   285 CITATIONS

SEE PROFILE

Some of the authors of this publication are also working on these related projects:

Air Sea Interaction in the Northern Indian Ocean View project

Transient enhancement and decoupling of carbon export vs opal in cyclonic eddies: overprints of submesoscale interactions and eddy evolution View project

Probability Distribution of Turbulent Kinetic Energy Dissipation Rate in Ocean: Observations and Approximations

I. Lozovatsky[1] [iD] **, H. J. S. Fernando[1,2]** [iD] **, J. Planella-Morato[1,3], Zhiyu Liu[4]** [iD] **, J.-H. Lee[5]** [iD] **, and S. U. P. Jinadasa[6]**

[1]Environmental Fluid Dynamics Laboratories, Department of Civil and Environmental Engineering and Earth Sciences, University of Notre Dame, Notre Dame, IN, USA, [2]Department of Aerospace and Mechanical Engineering, University of Notre Dame, Notre Dame, IN, USA, [3]Department of Physics, University of Girona, Girona, Catalonia, Spain, [4]State Key Laboratory of Marine Environmental Science, and Department of Physical Oceanography, College of Ocean and Earth Sciences, Xiamen University, Xiamen, China, [5]Physical Oceanography Division, Korean Institute of Ocean Science and Technology, Ansans-si, Gyeonggi-do, Korea, [6]Department of Physical Oceanography, National Aquatic Resources Research and Development Agency, Crow Island, Colombo, Sri Lanka

Abstract The probability distribution of turbulent kinetic energy dissipation rate in stratified ocean usually deviates from the classic lognormal distribution that has been formulated for and often observed in unstratified homogeneous layers of atmospheric and oceanic turbulence. Our measurements of vertical profiles of micro-scale shear, collected in the East China Sea, northern Bay of Bengal, to the south and east of Sri Lanka, and in the Gulf Stream region, show that the probability distributions of the dissipation rate $\tilde{\varepsilon}_r$ in the pycnoclines ($r \sim 1.4$ m is the averaging scale) can be successfully modeled by the Burr (type XII) probability distribution. In weakly stratified boundary layers, lognormal distribution of $\tilde{\varepsilon}_r$ is preferable, although the Burr is an acceptable alternative. The skewness Sk_ε and the kurtosis K_ε of the dissipation rate appear to be well correlated in a wide range of Sk_ε and K_ε variability.

Plain Language Summary The probability distribution of turbulent kinetic energy dissipation rate in stratified ocean usually deviates from the classic lognormal distribution that has been formulated for and often observed in homogeneous layers of atmospheric and oceanic turbulence. Our microstructure measurements, collected in the East China Sea, northern Bay of Bengal, to the south and east of Sri Lanka, and in the Gulf Stream region, show that the probability distributions of the dissipation rate in stably stratified layers can be successfully modeled by the Burr (type XII) probability distribution. In weakly stratified boundary layers, lognormal distribution of the dissipation is preferable, although the Burr is an acceptable alternative.

1. Introduction

Ocean turbulence is highly intermittent in space and time (e.g., Seuront et al., 2005) with characteristic vertical scales of turbulent zones (patches) varying from several centimeters up to tens of meters. Turbulent patches are randomly generated and decayed in stratified ocean, being usually quantified by the turbulent kinetic energy (TKE) dissipation rate $\tilde{\varepsilon}_r$ averaged over particular volumes or radius r. The patchiness of ocean turbulence (or its spatial inhomogeneity) has been defined as the "mesoscale" or "external" intermittency of $\tilde{\varepsilon}_r$ (Lozovatsky et al., 2010), which is to be distinguished from the "internal" or genuine intermittency of the dissipation rate. The latter is attributed to random distribution of vortex filaments within turbulent regions, where they stretch and dissipate energy in isolation (Kuo & Corrsin, 1971). Internal intermittency characterizes fluctuations of $\tilde{\varepsilon}_r$ in the inertial-convective subrange (Tennekes & Lumley, 1972), between an outer turbulent scale L_0, which is typically about 1 m in the oceanic pycnocline, and a dissipative scale $L_K \sim 40\eta_K$ (Gregg et al., 1996), where $\eta_K = (v^3/\varepsilon)^{1/4}$ is the Kolmogorov scale (Monin & Yaglom, 1975) and v the molecular viscosity. This is the essence of the refined similarity hypothesis (RSH) proposed by Kolmogorov (1962) and Obukhov (1962), wherein lognormal distribution for $\tilde{\varepsilon}_r$ was suggested. Considering random multiplicative cascade of turbulent eddies, generated at outer scales of turbulence, toward smaller scales of the dissipation, Gurvich and Yaglom (1967) formulated the first model of turbulence

Table 1
The Sites of Dissipation Measurements in 2005–2015

Station name and dates	Latitude (φ) and longitude (λ)	Water depth (m)	Duration (h), profiler, number of cast
East China Sea (R/V *Eardo*, S. Korea)			
IEODO: 27 Aug 2005	$\varphi = 32.12°N$, $\lambda = 125.17°E–125.19°E$	41–50	5.5, 57 TurboMAP casts
IEODO: 13–14 Aug 2006	$\varphi = 32.13°N–32.18°N$, $\lambda = 125.17°E$	49–63	20, 134 TurboMAP casts
East China Sea (R/V *Beidou*, China)			
CDW: 3–4 Sep 2006	$\varphi = 30.82°N$, $122.93°E$	38	25, 50 MSS casts
S1: 20–21 Sep, 2006	$\varphi = 35.01°N$, $\lambda = 123.00°E$	73	25, 71 MSS casts
S2: 25–26 Sep 2006	$\varphi = 35.00°N$, $\lambda = 121.50°E$	37	25, 78 MSS casts
Northern Bay of Bengal (R/V *Roger Revelle*, USA); Weligama (WS) and Trincomalee (TS) sections from Sri Lankan coast (R/V *Samuddrika*, SrL)			
BoB1: 18 Nov 2013	$\varphi = 15.94°N–15.96°N$, $\lambda = 86.94.3°E–86.96°E$	2,740	1.5, 12 VMP casts
BoB2: 19 Nov 2013	$\varphi = 15.95°N$, $\lambda = 86.91°E–86.94°E$	2,750	1.5, 12 VMP casts
BoB3: 21 Nov 2013	$\varphi = 16.20°N–16.22°N$, $\lambda = 86.96°E$	2,690	2, 12 VMP casts
BoB4: 23 Nov 2013	$\varphi = 15.95°N–16.18°N$, $\lambda = 86.72°E–86.91°E$	2,740	5.5, 12 VMP casts
WS: 23–24 Apr 2014	$\varphi = 5.92°N–5.37°N$, $\lambda = 80.4°E$	120–4,200	19, 16 VMP casts
WS/drift: 25 Apr 2014	$\varphi = 5.73°N$, $\lambda \sim 80.45°E$	1,200–1,240	4, 18 VMP casts
TS: 9–10 Sep 2014	$\varphi = 8.0°N–8.1°N$, $\lambda = 81.79°E–82.6°E$	960–3,870	20, 19 VMP casts
Gulf Stream region to the east of the NC shelf (R/V *Atlantic Explorer*, USA)			
GS_S: 30 Oct 2015	$\varphi = 35.83°N$, $\lambda = 74.10°E$	2,660	2, 4 VMP casts
GS_N: 1 Nov 2015	$\varphi = 36.17°N$, $\lambda = 74.54°E$	1,670–1,770	2, 5 VMP cast
	$\varphi = 36.14°N$, $\lambda = 74.51°E$		
R56: 1 Nov 2015	$\varphi = 36.24°N$, $\lambda = 74.76°E$	720	1, 3 VMP casts

intermittency, which led to lognormal distribution of $\tilde{\varepsilon}_r$ in agreement with RSH. Although the lognormal model and its modifications (e.g., Yamazaki, 1990) have been successfully applied to various high Reynolds numbers turbulent flows, they appear to be mathematically ill posed (e.g., Mandelbrot 1974; Novikov, 1970). It is because the central-limit theorem is not applicable to rare but powerful turbulent events that contribute the most to high-order moments of the velocity increments. Therefore, the distribution of $\log \varepsilon$ cannot be
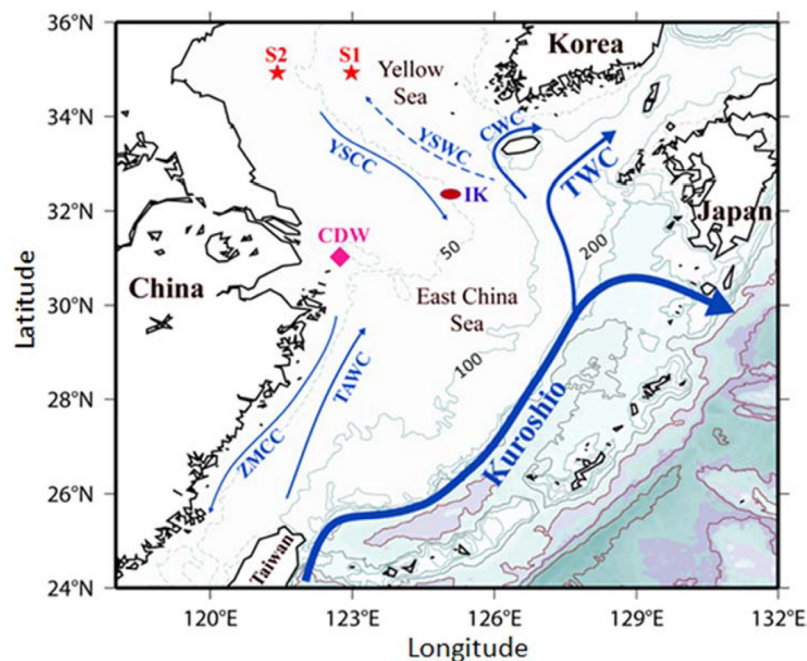
Figure 1. Bathymetry and main patterns of circulation in the East China Sea and Yellow Sea based on Zhang et al. (2016) and Lie and Cho (2016): TWC, Tsushima Warm Current; TAWC, Taiwan Warm Current; YSCC, Yellow Sea Coastal Current; YSWC, Yellow Sea Warm Current; CWC, Cheju Warm Current; ZMCC, Zhe-Min Coastal Current. Measurements at stations S1 and S2 (Liu et al., 2009) and at CDW (Lozovatsky et al., 2012) were taken in 2006 using an MSS-60 profiler; measurements at IK site (Lozovatsky, Jinadasa, et al., 2015; Lozovatsky, Lee, et al., 2015) were conducted in 2005 and 2006 using a TurboMAP profiler.

Table 2

Parameters of the Burr and Lognormal Distributions Used to Fit the CDF(ε) From the Northern Bay of Bengal (BoB) and Around Sri Lanka (WS, WDr, TS)

No	Approximation region, dates, layers, number of samples (n)	Burr distribution α	c	k	Mean, median, mode	Lognormal distribution μ	σ	Mean, median, mode	ℓ = log likelihood Burr/ lognormal	Empirical estimates mean, median, mode
20	BoB, 18 Nov, PC (n = 778), z > 20 m	6.4×10^{-10}	3.65	0.47	1.44×10^{-9}, 8.93×10^{-10}, 6.36×10^{-10}	−20.75	0.75	1.30×10^{-9}, 9.7×10^{-10}, 5.5×10^{-10}	**15,324**/15,260	1.51×10^{-9}, 8.9×10^{-10}, 4.0×10^{-10}
21	BoB, 19 Nov, PC (n = 781), z > 25 m	3.7×10^{-10}	3.30	0.34	3.35×10^{-9}, 6.6×10^{-10}, 3.8×10^{-10}	−20.98	1.02	1.30×10^{-9}, 7.7×10^{-10}, 2.7×10^{-10}	**15,353**/15,263	2.50×10^{-9}, 6.5×10^{-10}, 1.4×10^{-10}
22	BoB, 21 Nov, PC (n = 589), z > 55 m	2.9×10^{-10}	3.02	0.51	7.7×10^{-10}, 4.1×10^{-10}, 2.7×10^{-10}	−21.52	0.85	6.4×10^{-10}, 4.5×10^{-10}, 2.2×10^{-10}	**11,982**/11,941	9.7×10^{-10}, 4.3×10^{-10}, 2.5×10^{-10}
23	BoB, 23 Nov, PC (n = 727), z > 50 m	1.5×10^{-10}	4.65	0.22	3.76×10^{-9}, 3.0×10^{-10}, 1.7×10^{-10}	−21.70	1.00	6.2×10^{-10}, 3.8×10^{-10}, 1.4×10^{-10}	**14,851**/14,748	8.3×10^{-10}, 2.9×10^{-10}, 2.1×10^{-10}
24	WDr, PC (n = 1,050), z > 30 m	4.4×10^{-10}	3.32	0.28	-, 9.0×10^{-10}, 4.7×10^{-10}	−20.60	1.14	2.16×10^{-9}, 1.13×10^{-9}, 3.1×10^{-10}	**20,104**/20,002	2.75×10^{-9}, 8.8×10^{-10}, 1.9×10^{-10}
25	WS, PC (n = 1,099), z > 30 m	3.9×10^{-10}	3.71	0.23	-, 8.67×10^{-9}, 4.32×10^{-9}	−20.60	1.20	2.32×10^{-9}, 1.13×10^{-9}, 2.7×10^{-10}	**21,023**/20,880	3.47×10^{-9}, 8.4×10^{-10}, 7.3×10^{-10}
26	TS, PC (n = 575), z > (10–30) m	4.8×10^{-10}	3.33	0.23	-, 1.17×10^{-9}, 5.2×10^{-10}	−20.24	1.30	3.78×10^{-9}, 1.62×10^{-9}, 3.0×10^{-10}	**10,719**/10,670	4.99×10^{-9}, 1.15×10^{-9}, 1.3×10^{-10}

Note. PC refers to the pycnocline depths exceeding given z; n is the number of samples used to calculate CDF(ε). A larger log likelihood estimate is in bold. The respective CDF(ε) plots are shown in Figure 4.

normal (e.g., Moum & Rippeth, 2009; Seuront, 2008). Yet many researchers regard lognormal distribution as a good practical approximation for $\tilde{\varepsilon}_r$ that characterizes internal/genuine intermittency of turbulence generated either continuously or by individual events/overturns (see Frisch, 1995, for an extensive discussion).

Table 3

Parameters of the Burr and Lognormal Distributions Used to Approximate the CDF(ε) for the Gulf Stream Region and Adjoining Waters

No	Approximation region, dates, layers, number of samples (n)	Burr distribution α	c	k	Mean, median, mode	Lognormal distribution μ	σ	Mean, median, mode	ℓ = log likelihood Burr/ lognormal	Empirical estimates mean, median, mode
29	GS-S, 10 A.M., PC (n = 436), z > 60 m	1.27×10^{-9}	18.5	0.08	3.91×10^{-9}, 2.03×10^{-9}, 1.54×10^{-9}	−19.8	0.66	3.13×10^{-9}, 2.51×10^{-9}, 1.63×10^{-9}	**8,307**/8,195	3.35×10^{-9}, 1.98×10^{-9}, 1.05×10^{-9}
30	GS-N, 10 A.M., PC (n = 314), z > 10 m	1.85×10^{-9}	19.3	0.06	1.25×10^{-8}, 3.41×10^{-9}, 2.4×10^{-9}	−19.26	0.93	6.66×10^{-9}, 4.32×10^{-9}, 1.82×10^{-9}	**5,755**/5,626	1.01×10^{-8}, 3.32×10^{-9}, 1.60×10^{-9}
31	GS-N, 8–9 P.M., PC (n = 646), z > 30 m	1.66×10^{-9}	8.96	0.10	-, 3.49×10^{-9}, 2.65×10^{-9}	−19.17	0.94	7.39×10^{-9}, 4.74×10^{-9}, 1.96×10^{-9}	**11,591**/11,504	1.25×10^{-8}, 4.05×10^{-9}, 1.05×10^{-9}
32	R56, 6 P.M., PC (n = 490), z > 10 m	1.9×10^{-9}	10.96	0.14	5.42×10^{-9}, 2.98×10^{-9}, 2.48×10^{-9}	−19.46	0.67	4.45×10^{-9}, 3.56×10^{-9}, 2.27×10^{-9}	**9,155**/9,035	5.08×10^{-9}, 2.87×10^{-9}, 1.24×10^{-9}

Note. PC refers to the pycnocline depths exceeding given z; n is the number of samples used to calculate CDF(ε). A larger log likelihood estimate is in bold. The respective plots are shown in Figure 5.

Table 4

Parameters of the Burr and Lognormal Fits of Empirical CDF(ε) for Several Regions of the East China Sea (ECS)

No	Approximation region, dates, layers, number of samples (n)	Burr distribution parameters				Lognormal distribution parameters			ℓ = log likelihood Burr/ lognormal	Empirical estimates mean, median, mode
		α	c	k	Mean, median, mode	μ	σ	Mean, median, mode		
3	ECS, 2005, IEODO, PC (n = 616), 15 < z < 25 m	56.7×10^{-9}	1.09	1.34	1.29×10^{-7}, 3.97×10^{-8}, 2.73×10^{-9}	-17.09	1.46	1.1×10^{-7}, 3.78×10^{-8}, 4.49×10^{-9}	9,413/**9,421**	1.07×10^{-7}, 3.93×10^{-8}, 9.5×10^{-10}
4	ECS, 2005, IEODO, BL (n = 243), 40 < z < 54 m	130×10^{-9}	1.93	0.99	2.15×10^{-7}, 1.31×10^{-7}, 7.2×10^{-8}	-15.85	0.94	2.03×10^{-7}, 1.31×10^{-7}, 5.40×10^{-8}	**3,524**/3,521	2.08×10^{-7}, 1.37×10^{-7}, 1.98×10^{-7}
5	ECS, 2006, IEODO, PC (n = 2,140), 13 < z < 30 m	9.83×10^{-9}	1.81	0.54	-, 1.67×10^{-8}, 3.45×10^{-8}	-17.76	1.32	4.63×10^{-8}, 1.94×10^{-8}, 3.39×10^{-9}	34,432/34,377	6.72×10^{-8}, 1.69×10^{-8}, 1.04×10^{-8}
6	ECS, 2006, IEODO, BL (n = 2,090), 40 < z < 63 m	714×10^{-9}	0.77	3.21	3.29×10^{-7}, 1.12×10^{-7}, -	-16.22	1.81	4.65×10^{-7}, 9.03×10^{-8}, 3.41×10^{-9}	29,730/29,684	3.39×10^{-7}, 1.24×10^{-7}, 1.11×10^{-7}
7	ECS, 2006, CDW, PC (n = 390), 10 < z < 25 m	4.74×10^{-9}	2.01	0.51	1.92×10^{-7}, 8.04×10^{-9}, 3.35×10^{-9}	-18.50	1.19	1.88×10^{-8}, 9.24×10^{-9}, 2.24×10^{-9}	**6,597**/6,594	2.02×10^{-8}, 8.44×10^{-9}, 1.11×10^{-8}
8	ECS, 2006, CDW, BL (n = 287), 25 < z < 37 m	15.5×10^{-9}	1.56	0.64	-, 2.38×10^{-8}, 6.86×10^{-9}	-17.45	1.37	6.75×10^{-8}, 2.64×10^{-8}, 4.04×10^{-9}	**4,513**/4,511	8.06×10^{-8}, 2.48×10^{-8}, 1.21×10^{-8}
10	ECS, 2006, S1, PC (n = 894), 18 < z < 31 m	7.21×10^{-9}	1.50	0.68	3.64×10^{-7}, 1.06×10^{-8}, 2.84×10^{-9}	-18.28	1.37	2.94×10^{-8}, 1.15×10^{-8}, 1.76×10^{-9}	14,787/**14,793**	3.09×10^{-8}, 1.05×10^{-8}, 1.05×10^{-9}
11	ECS, 2006, S1, BL (n = 2,021), 35 < z < 72 m	0.36×10^{-9}	2.31	0.33	-, 8.44×10^{-10}, 3.17×10^{-10}	-20.61	1.42	4.07×10^{-9}, 1.12×10^{-9}, 1.5×10^{-10}	**38,187**/38,063	4.33×10^{-9}, 8.9×10^{-10}, 1.27×10^{-9}
13	ECS, 2006, S2, PC (n = 178), 15 < z < 24 m	63.1×10^{-9}	0.82	2.70	4.04×10^{-8}, 1.41×10^{-8}, -	-18.23	1.65	4.72×10^{-8}, 1.21×10^{-8}, 7.9×10^{-10}	2,902/**2,904**	3.69×10^{-8}, 1.39×10^{-8}, 1.58×10^{-9}
14	ECS, 2006, S2, BL (n = 316), 25 < z < 37 m	274×10^{-9}	1.84	1.80	2.37×10^{-7}, 1.82×10^{-7}, 1.13×10^{-7}	-15.58	0.85	2.46×10^{-7}, 1.71×10^{-7}, 8.32×10^{-8}	**4,535**/4,526	2.40×10^{-7}, 1.88×10^{-7}, 1.75×10^{-7}

Note. PC and BL refer to the pycnocline and bottom layer depths z, respectively, which are specified; n is the number of samples used to calculate CDF(ε). The respective CDF(ε) plots are shown in Figures 6 and 7.

Yamazaki and Lueck (1990) demonstrated that lognormal model can be applied to $\tilde{\varepsilon}_r$, if turbulence is statistically homogeneous in a particular region with the averaging scale $L_K \ll r \ll L_0$, which is viable in well-mixed relatively thick turbulent boundary layers below the sea surface and above the ocean floor (e.g., Lozovatsky et al., 2010) and in large turbulent overturns (~10 m or more in height) that are from time to time observed in the ocean interior (e.g., Gregg et al., 1993; Hebert et al., 1992; Peters et al., 1995; Wijesekera et al., 1993). However, in strongly stratified pycnoclines, large turbulent patches are rare events. Therefore, conventional equidistant estimates of $\tilde{\varepsilon}_\varsigma$, which are usually calculated over relatively small vertical domains (typical averaging distance $\varsigma = 1–2$ m), represent a random field of dissipation samples observed at various stages of turbulence evolution. The probability distributions of this dissipation field in a specific region can characterize external/mesoscale intermittency of turbulence influenced by larger scale dynamical processes, which depend on energy sources and ambient stratification.

As has already been mentioned, the probability distributions of $\tilde{\varepsilon}_\varsigma$ were found to be close to lognormal in boundary layers or large well-mixed layers in the pycnocline, where the basic limitation, $L_K \ll r \ll L_0$, of Gurvich and Yaglom (1967) is met (e.g., Baker & Gibson, 1987; Moum et al., 1989; Wijesekera et al., 1993; Yamazaki & Lueck, 1990). However, it has recently been shown (Lozovatsky, Jinadasa, et al., 2015; Lozovatsky, Lee, et al., 2015) that the probability distribution of the logarithm of the dissipation rate $\log_{10} \tilde{\varepsilon}_\varsigma$ ($\varsigma \sim 1.4$ m) in strongly stratified pycnocline can follow the generalized extreme value distribution (Kotz & Nadarajah, 2000) given the

Table 5

Parameters of the Burr and Lognormal Approximations of the CDF(ε) Pertained to the Specified Surface Mixed Layer (ML) Depths in the Bay of Bengal (BoB), Near Sri Lanka (WDr), and in the Gulf Stream (GS-S)

Approximation region, dates, layers, number of samples (n)	Burr distribution				Lognormal distribution			log likelihood Burr/ lognormal	Empirical estimates mean, median, mode
	α	c	k	Mean, median, mode	μ	σ	Mean, median, mode		
BoB, Nov 19, ML (n = 177), 10 < z < 30 m	$4.9{\times}10^{-8}$	0.69	1.00	- $4.9{\times}10^{-8}$, -	−16.82	2.51	$1.16{\times}10^{-6}$, $4.96{\times}10^{-8}$, $9.1{\times}10^{-11}$	2,560/**2,563**	$7.12{\times}10^{-7}$, $5.09{\times}10^{-8}$, $2.3{\times}10^{-10}$
BoB, Nov 21, ML (n = 117), 10 < z < 45 m	$1.97{\times}10^{-8}$	1.25	0.94	$1.18{\times}10^{-7}$, $2.11{\times}10^{-8}$, $2.62{\times}10^{-8}$	−17.66	1.47	$6.28{\times}10^{-8}$, $2.14{\times}10^{-8}$, $2.47{\times}10^{-9}$	1,856/**1,856**	$5.38{\times}10^{-7}$, $2.27{\times}10^{-8}$, $5.9{\times}10^{-10}$
BoB, Nov 23, ML (n = 187), 15 < z < 45 m	$1.8{\times}10^{-10}$	2.89	0.17	- $6.8{\times}10^{-10}$, $1.9{\times}10^{-10}$	−20.43	1.99	$9.70{\times}10^{-9}$, $1.34{\times}10^{-9}$, $2.6{\times}10^{-11}$	**3,454**/3,427	$1.87{\times}10^{-8}$, $7.7{\times}10^{-10}$, $5.9{\times}10^{-11}$
WDr, ML (n = 193), 10 < z < 30 m	$1.03{\times}10^{-8}$	1.37	1.48	$1.29{\times}10^{-8}$, $7.07{\times}10^{-9}$, $2.22{\times}10^{-9}$	−18.82	1.11	$1.24{\times}10^{-8}$, $6.71{\times}10^{-9}$, $1.96{\times}10^{-9}$	3,334/**3,339**	$1.19{\times}10^{-8}$, $6.76{\times}10^{-9}$, $5.9{\times}10^{-10}$
GS-S, 10 A.M., ML (n = 201), 10 < z < 59 m	$2.77{\times}10^{-8}$	1.46	1.15	$5.12{\times}10^{-8}$, $2.43{\times}10^{-8}$, $2.12{\times}10^{-8}$	−17.55	1.14	$4.58{\times}10^{-8}$, $2.39{\times}10^{-8}$, $6.53{\times}10^{-9}$	3,213/**3,216**	$4.61{\times}10^{-8}$, $2.14{\times}10^{-8}$, $2.27{\times}10^{-9}$

Note. The respective *CDF*(ε) plots are shown in Figure 9; *n* is the number of samples used to calculate *CDF*(ε).
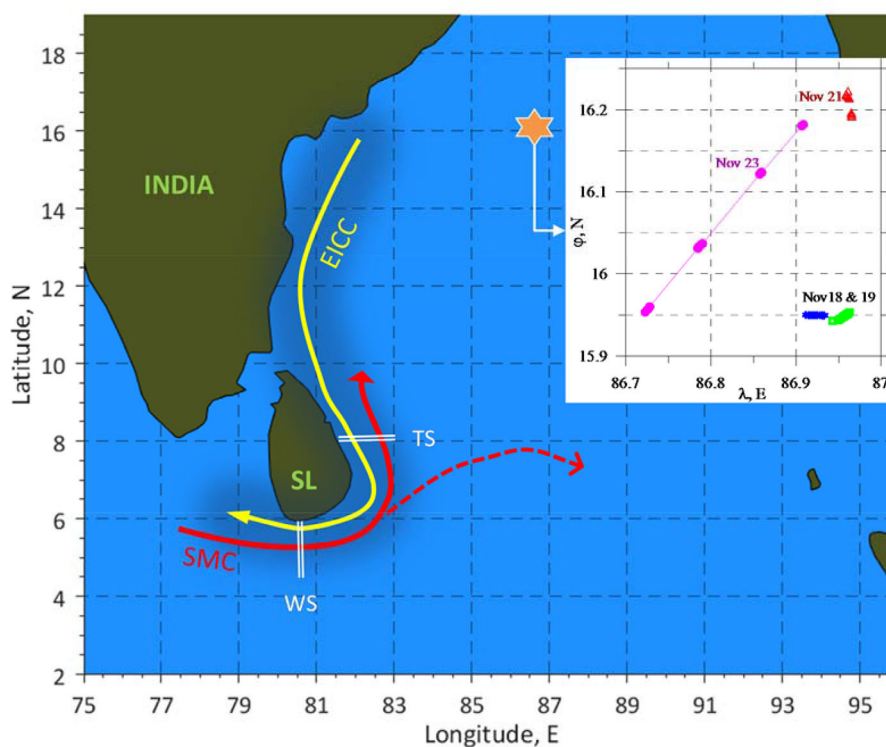

Figure 2. The VMP measurements in the northern Bay of Bengal (the orange star shows the location of measurements using R/V *Roger Revelle*, November 2013) and along the Weligama (WS) and Trincomalee (TS) sections (R/V *Samuddrika*, April and September 2014, respectively). The main currents in the region are the East Indian Coastal Current (EICC) with its extension to the south of Sri Lanka as the Winter Monsoon Current (yellow arrow) and the South Monsoon Current (SMC) with the main (red arrow) and a secondary (dashed arrow) branches directed northward and eastward, respectively.

rare, random generation of energetic turbulence events that form patches of high dissipation rate, while most of the background turbulence is confined to weakly dissipative regions that are at final stages of turbulence decay. Random patches of intense turbulence may affect tails of the dissipation rate probability distribution (Cuypers et al., 2012; Rousseau et al., 2010), making them heavier than the exponential bounds. The distribution tails (especially long/fat tails) can be characterized by skewness and kurtosis of the random variable (Rachev et al., 2010), providing direct link between those statistical parameters as well as external and internal intermittency of turbulence (Moum & Rippeth, 2009; Thorpe et al., 2008).

This paper tests the hypothesis that the probability distribution of the TKE dissipation rate in stratified ocean measured by airfoil sensors substantially deviates from the classic lognormal approximation and often follows the Burr XII distribution (e.g., Burr, 1942; Okasha & Matter, 2015; Zimmer et al., 1998). We analyzed data from several field campaigns carried out by the authors during the last decade. Various statistics of the dissipation rate in the ocean, including its third and fourth moments are discussed. The measurements have been taken in the East China Sea, northern Bay of Bengal, to the south and east of Sri Lanka, and in the Gulf Stream region to the east of the North Carolina shelf.

2. Measurements

The measurements of $\tilde{\varepsilon}_{\varsigma}$ (hereinafter just ε) were collected between 2005 and 2015 during seven research cruises. In the East China Sea (ECS), one cruise was in 2005 and two in 2006. In the northern Bay of Bengal (BoB), one cruise was in 2013 and two were in 2014 to the south and to the east of Sri Lanka (SL). In 2015, the measurements in the Gulf Stream region (GS) were to the east of the North Carolina shelf break (one cruise).

Three commercially manufactured microstructure profilers that are commonly employed by the oceanographic community were used during the field campaigns. In the ECS (Liu et al., 2009; Lozovatsky et al., 2012; Lozovatsky, Jinadasa, et al., 2015; Lozovatsky, Lee, et al., 2015), we operated the MSS-60 profiler (Prandke & Stips, 1998) and TurboMAP (Wolk et al., 2002), while in BoB/SL (Jinadasa et al., 2016; Wijesekera et al., 2016) and in GS (Lozovatsky et al., 2017), the measurements were taken by VMP-500 (http://rocklands-cientific.com/products/profilers/vmp-500/). In shallow waters (ECS) the measurements were collected in the depth range between the sea surface and 1–3 m above the sea floor; and in deep waters (BoB/SL and GS) the profilers descended to ∼130–150 m, being limited by the length of a tethered cable and weather condi-

Figure 3. The Google Earth topography in the region of VMP measurements off the North Carolina shelf, showing the locations of the southern GS_S station (the red rectangular: $\varphi = 35.83°$N, $\lambda = 74.1°$W) near the Gulf Stream core, the northern GS_N station (the white crossed ellipse: $\varphi = 36.15°$N, $\lambda = 74.53°$W) near the GS northern wall, and R56 station near the shelf break (the red-yellow star: $\varphi = 36.25°$N, $\lambda = 74.76°$W).

tions. Note that microstructure data uncontaminated by the ship movement could be obtained starting ∼3–5 m below the sea surface. During rough weather conditions, the upper 5–10 m of the dissipation $\varepsilon(z)$ profiles were removed from analysis. Table 1 summarizes the data sets used in this study; measurement locations are shown in Figures 1 (ESC), 2 (BoB/SL), and 3 (GS).

All microstructure profilers carried two airfoil probes (to measure microscale shear for ε estimation), a three-component accelerometer, pressure sensor (depth) and a temperature-conductivity package for temperature, salinity, and potential density (our VMP-500 was equipped with a precise Sea-Bird unit). The data processing followed the methodology of Roget et al. (2006); for more information, see Liu et al. (2009) and Lozovatsky, Lee, et al. (2015). The TKE dissipation rate ε was calculated by fitting Nasmyth or Panchev-Kesich benchmark spectra to the measured shear spectrum (e.g., Gregg, 1999) over consecutive segments of 2 s (1,024 points). As a result, vertical profiles of $\varepsilon(z)$ were obtained with a vertical spacing of ∼1.2–1.5 m (1.4 on the average). The same spacing was adopted for temperature $T(z)$, salinity $S(z)$, and specific potential density $\sigma_\theta(z)$ profiles. The squared buoyancy frequency $N^2(z)$ was calculated using the rearranged $\sigma_\theta(z)$ wherein potential density monotonically increases with depth.

Our analysis is mostly focused on data belonging to the ocean pycnocline. In shallow waters, this is defined as a stably stratified layer that underlies the near surface mixed layer (ML) and overlies the near
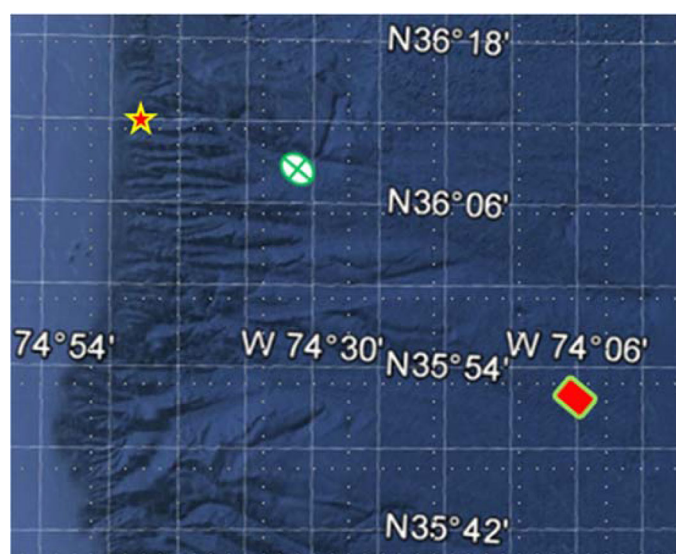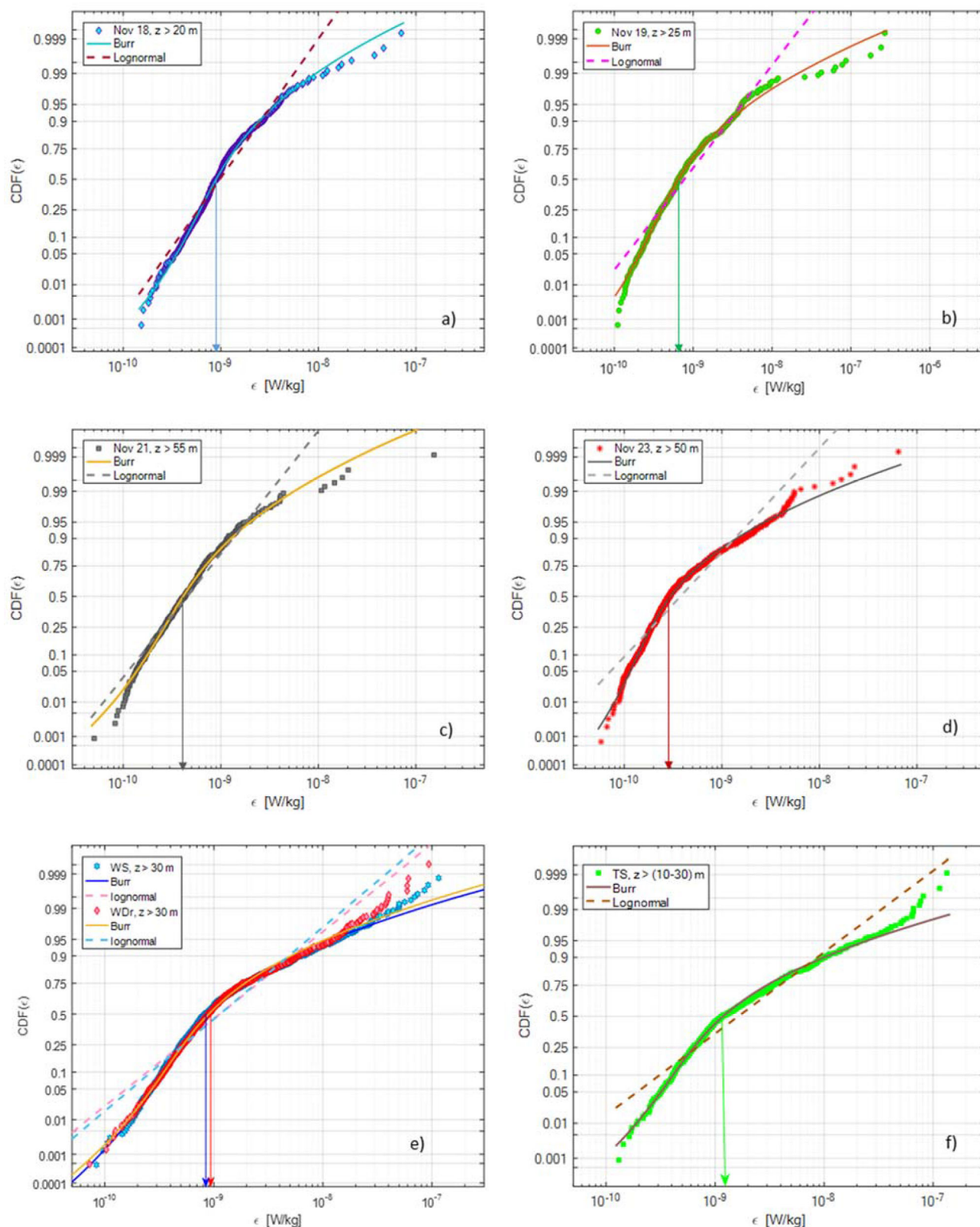
Figure 4. The cumulative distribution functions $CDF(\varepsilon)$ for the BoB and SL pycnocline dissipation rate ε_{pc} in the depth ranges between the pycnocline upper boundaries shown in the legends and $z = \sim130$ m. The BoB data of 2013: (a) 18 November, (b) 19 November, (c) 21 November, and (d) 23 November. The SL data: Weligama section (WS), (e) Weligama drift (WDr) and (f) Trincomalee section (TS). CDF are approximated by the Burr and lognormal distributions; the less favorable approximation among the two is shown by dash lines; the arrows point to the medians. Parameters of the distributions are in Table 2.

bottom mixed layer (BL). In several cases, when the amount of $\varepsilon(z)$ samples from the BL and ML (below $z = 5$–10 m) is substantial, cumulative distribution functions $CDF(\varepsilon)$ were also computed and analyzed.

3. The Dissipation Rate Statistics

3.1. Rationale for Using Burr Probability Distribution Versus Lognormal Distribution for $CDF(\varepsilon)$

As mentioned, the most widely used model for probability distribution of ε is the lognormal one (Gurvich & Yaglom, 1967), with the cumulative distribution function

$$CDF_{\ln}(\varepsilon) = \Phi\left(\frac{\ln \varepsilon - \mu_{\ln \varepsilon}}{\sigma_{\ln \varepsilon}}\right), \tag{1}$$

where Φ is the CDF of the standard normal distribution (Krishnamoorthy, 2006) of the natural logarithm of ε. The log-scale $\mu_{\ln \varepsilon}$ and shape $\sigma_{\ln \varepsilon}$ parameters of the distribution determine the mean $\tilde{\varepsilon}$ and median $\hat{\varepsilon}$ values of the dissipation as
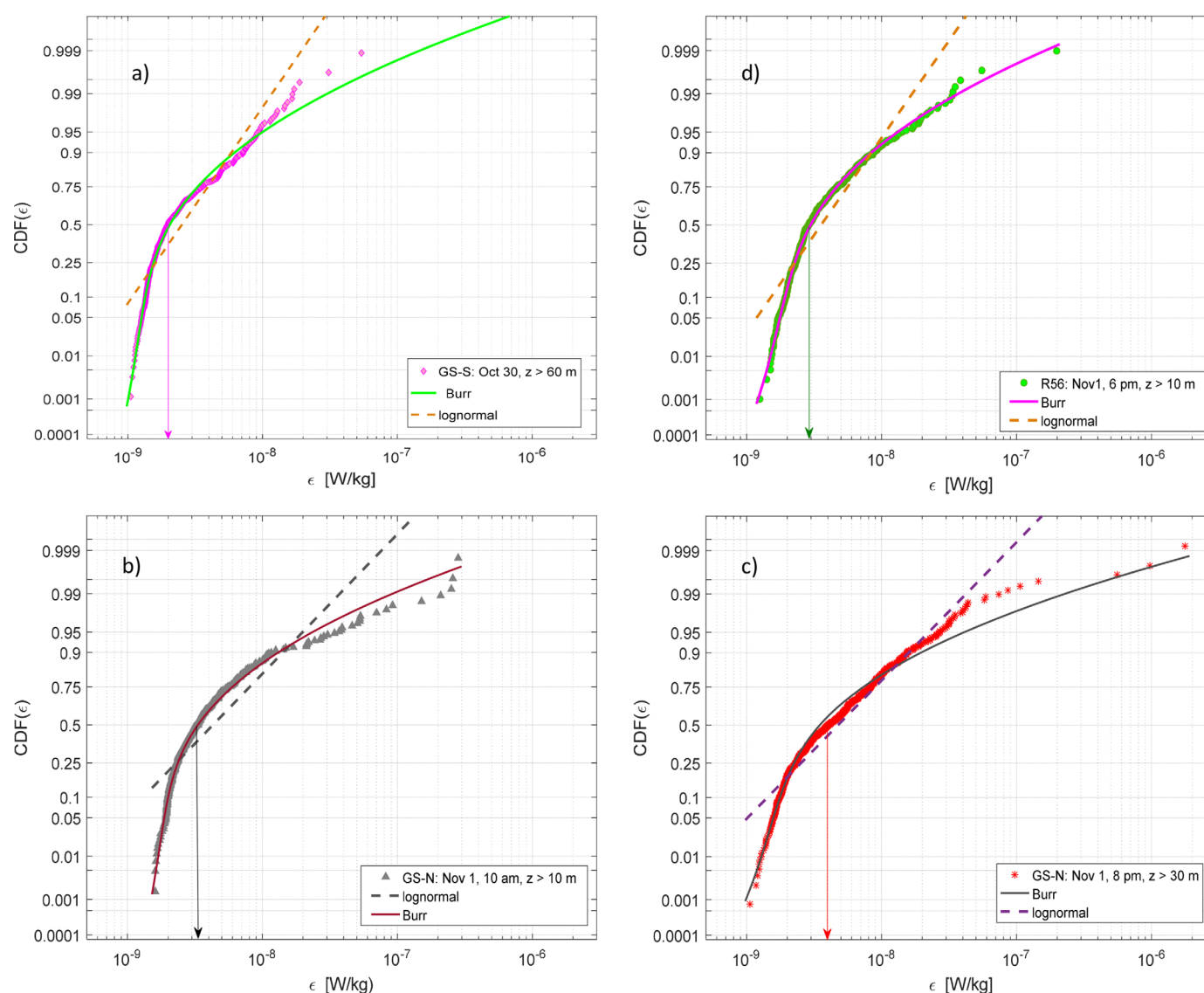
Figure 5. The cumulative distribution functions $CDF(\varepsilon)$ for the pycnocline dissipation rate ε_{pc} (above $z = \sim 130$ m) at (a) stations GS-S, (b) GS-N 10 A.M. and (c) GS-N 8–9 P.M., and (d) R56 approximated by the Burr and lognormal distributions (the pycnocline upper boundaries are given in the legends). Parameters of the distributions are in Table 3. The arrows point to the median values. The dash lines indicate the less favorable approximation of the two.
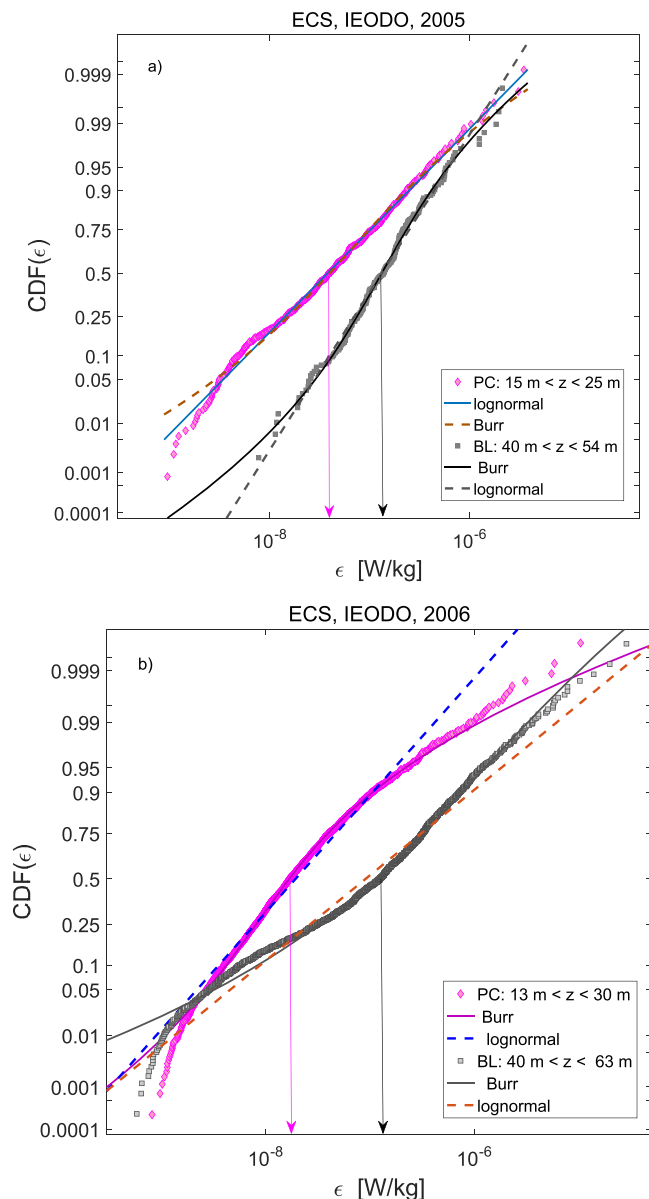
Figure 6. The cumulative distribution functions $CDF(\varepsilon)$ of the TKE dissipation rate ε for the pycnocline (PC) and bottom boundary layer (BL) in the central basin of the ECS to the south of Jeju Island near IEODO station (see Figure 1) for (a) 2005 and (b) 2006 measurements. Parameters of the Burr and lognormal approximations are in Table 4. The dash lines indicate less favorable approximation among the two, arrows are the medians. The depth ranges of PC and BL are given in legends.

$$\tilde{\varepsilon} = \exp\left(\mu_{\ln\varepsilon} + \sigma_{\ln\varepsilon}^2/2\right) \text{ and } \hat{\varepsilon} = \exp\left(\mu_{\ln\varepsilon}\right). \qquad (2)$$

It has been shown that empirical $CDF(\varepsilon)$ quite often deviates from the lognormal model, especially for pycnocline samples, such as those analyzed by Lozovatsky, Lee, et al. (2015), where the generalized extreme value (GEV) distribution was fitted to $CDF(\log_{10}\varepsilon)$. Note that both of these distributions have so-called right-side heavy tails (due to rare appearance of extremely large events), which means that the distribution tails are not exponentially bounded. The list of heavy tailed distributions includes such popular distributions as Weibull, gamma, and Pearson distributions (Tadikamalla, 1980), which are a part of the family of distributions introduced by Burr (1942). Here, we focus on the Burr type XII distribution (thereafter the Burr distribution) that has right-side algebraic tail, which is more effective for modeling distributions of rare events (extreme dissipations) that occur with lesser frequency than for models with exponential tails. The Burr distribution produces a wide range of skewness and kurtosis—which are conventional parameters for characterizing turbulence intermittency (e.g., Sreenivasan & Antonia 1997; Tsinober, 2001). The probability density (pdf) and cumulative distribution (CDF) functions of Burr distribution for the dissipation rate ε (>0) can be written as

$$pdf_B(\varepsilon) = \frac{ck}{\varepsilon_0}\left(\frac{\varepsilon}{\varepsilon_0}\right)^{c-1}\left(1+\left(\frac{\varepsilon}{\varepsilon_0}\right)\right)^{-(k+1)}, \qquad (3)$$

$$CDF_B(\varepsilon) = 1 - (1+(\varepsilon/\varepsilon_0)^c)^{-k}, \qquad (4)$$

where both $c > 0$ and $k > 0$ are shape parameters and $\varepsilon_0 \equiv \alpha$ (Okasha & Matter, 2015; Rodriguez, 1977) is a scale parameter. The mean, mode, and median of the Burr distribution are

$$\mu_B = \frac{\alpha\,\Gamma\left(\frac{1}{c}\right)\Gamma\left(k-\frac{1}{c}\right)}{c\,\Gamma(k)}, \qquad (5)$$

$$Mode_B = \alpha\left(\frac{c-1}{ck+1}\right)^{1/c}, \; ck > 1, \qquad (6)$$

$$Med_B = \alpha\left(2^{1/k}-1\right)^{1/c}, \qquad (7)$$

where Γ is the gamma function. The Burr cumulative distribution and survival functions are written in closed form, which simplifies the computation of the percentiles and the likelihood function of censored data (Zimmer et al., 1998). It is a valuable feature for statistical analysis of the dissipation rate because reliable estimates of ε in the ocean have been found in a wide, yet bounded range between $\left(\sim 10^{-11} \text{ to } 10^{-10}\right) < \varepsilon < \left(\sim 10^{-4} \text{ to } 10^{-5}\right)$ W/kg (e.g., Baumert et al., 2005). A lower and higher trusted values of ε have not been reported yet due to technical limitations of existing instruments.

The empirical $CDFs(\varepsilon)$ were calculated for the available data sets and approximated by lognormal and Burr distributions using the MATLAB dfittool application, which allowed testing of a variety of probability models including such alternatives as beta, gamma, generalized extreme value, stable, log-logistic and Weibull distributions. All of the distributions considered above have been previously used for modeling various statistical aspects of turbulent flows. Parameters of the lognormal and Burr models are given in Tables 2–5 for the ECS, BoB/SL, and GS regions (Figures 1–3), respectively, along with the estimates of the mean, mode, and median for the corresponding approximations and empirical data. To check which of the two competing statistical models fits the data better (in the sense of information entropy), we calculated the normalized Akaike information criterion (Akaike, 1974; Bozdogan, 1987)

$$AIC = [(1 + \ln(n))p - 2\ell]/n, \tag{8}$$

where p is the number of model parameters ($p = 2$ for lognormal and $p = 3$ for the Burr, respectively), ℓ the maximized value of the log likelihood function of the model calculated in the course of the fitting process, and n the sample size, all of which are included in Tables 2–5. It should be emphasized that ℓ for all distributions are positive and high because the values of ε in W/kg are very small (much below unity), which lead to high negative values of AIC (the model with smaller AIC provides the better approximation to a specified data set). Later, we use the difference between AIC for the Burr and lognormal approximations to indicate the better choice for a particular set of the dissipation samples.

3.2. The Burr and Lognormal Approximations for the Observed $CDF(\varepsilon)$

Details of microstructure data employed in this study as well as the descriptions of background hydrometeorological conditions, regional circulation and local stratification are reported in Jinadasa et al. (2016), Wijesekera et al. (2016), and Lozovatsky et al. (2017) for deep ocean measurements taken in the BoB/SL and GS,
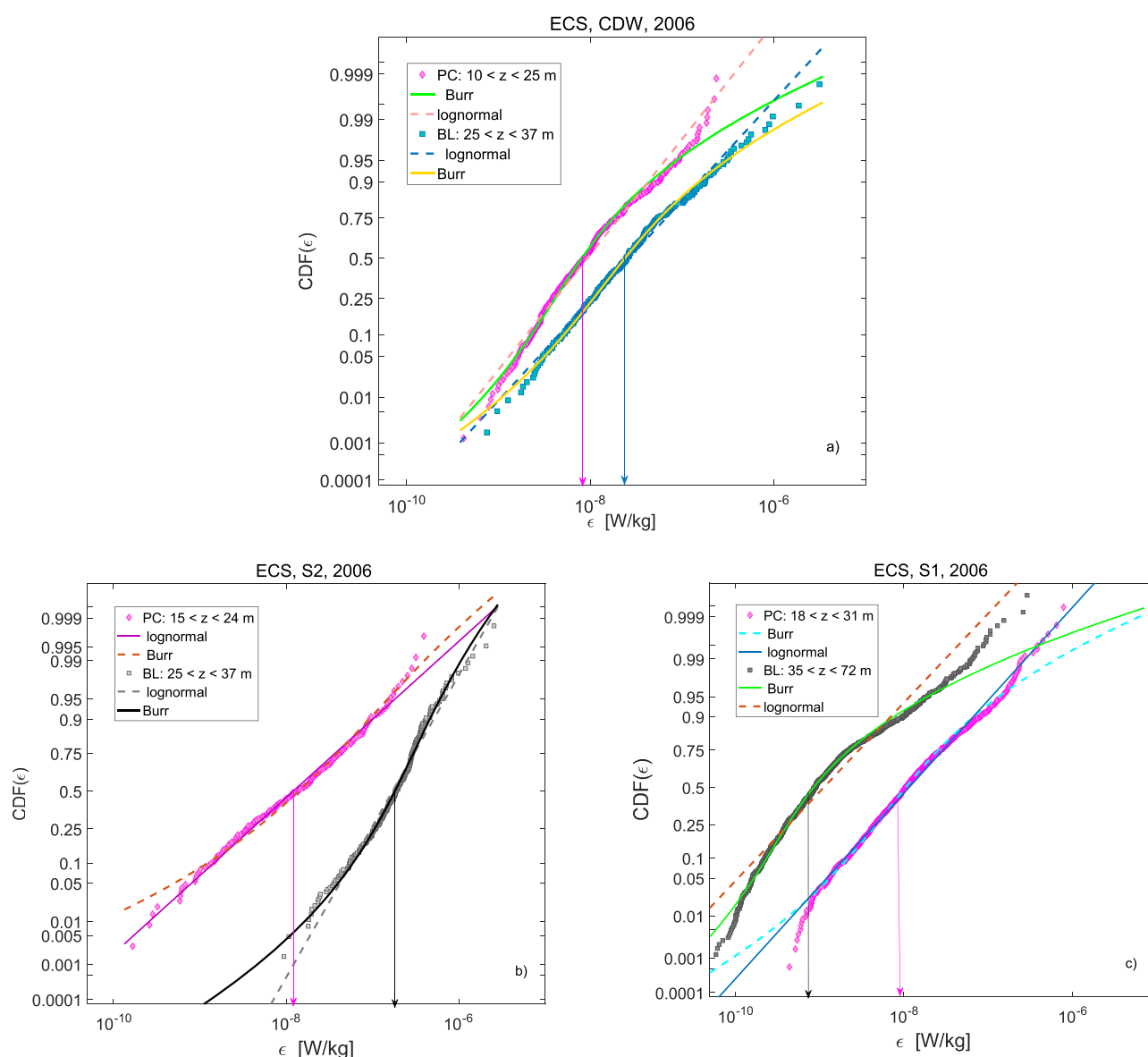

Figure 7. The cumulative distribution functions $CDF(\varepsilon)$ for the pycnocline (PC) and bottom layer (BL) near the inner shelf break of ECS at (a) CDW and (b) S2 stations, and in the central ECS at (c) station S1 (see Figure 1). The depth ranges of PC and BL are given in legends. Parameters of the Burr and lognormal approximations are in Table 4. The dash lines indicate the less favorable approximation among the two; the arrows point to the median values.

respectively, and by Liu et al. (2009), Lozovatsky et al. (2012), Lozovatsky, Lee, et al. (2015), and Lozovatsky, Jinadasa, et al. (2015) for shallow water measurements in the ECS.

The empirical cumulative distribution functions $CDF(\varepsilon)$ for the pycnocline (PC) depths in deep waters are shown in Figure 4 (northern Indian Ocean) and Figure 5 (Gulf Stream region), and information regarding these data sets, parameters of the distributions as well as parameters of the Burr and lognormal approximations are given in Tables 2 and 3. For shallow waters (ECS), the corresponding information is in Table 4 and in Figures 6 and 7. The preferable approximation between the two is always shown by solid line in Figures 4–7.

The Kolmogorov-Smirnov (K-S) nonparametric test (e.g., Massey, 1951) was used to verify the null hypothesis that empirical data come from the reference distribution (Burr or lognormal in our case) versus the alternative that they do not come from such a distribution. The result is 1 if the test rejects the null hypothesis at 0.05 significance level, or 0 otherwise; the corresponding p-values were also obtained (http://www.math-works.com/help/stats/kstest.html).

It appears, that the Burr model approximates 10 out of 11 empirical CDFs calculated for the GS and BoB/SL pycnocline measurements (Figures 4 and 5), while the lognormal model fails for all of these empirical distributions. The difference $\left(AIC_{Br} - AIC_{\lg n}\right)/n$ shown in Figure 8a for the Burr and Figure 8b for the lognormal models clearly indicate the suitability and dominance of the Burr model for strongly stratified ocean pycnocline.

In shallow waters (ECS), however, both models compete evenly to fit the data (the AIC differences in Figures 8a and 8b are close to zero), although the lognormal approximation fails three times more often than the Burr model (red stars versus red circle in the ECS panels). Note that four CDFs shown in Figures 6 and 7 (the corresponding AICs are marked as BL in Figure 8) belong to relatively tall (~10–20 m height), weakly stratified bottom layers of the central ECS, where the intermittency of ε resembles more that of a pycnocline rather than that of well-developed homogeneous turbulence in the surface mixing layer.

In this regard, several examples of the surface layer $CDF(\varepsilon)$ are shown in Figure 9 (details are in Table 5) for data obtained below $z = 10$ m in a well-defined mixed layers of at least 30–45 m deep (the BoB and SL/WDr measurements). According to Table 5 and results of the K-S test, the Burr model cannot be rejected for all the four empirical distributions, but for three of them the lognormal model also does well, if not even slightly better than the Burr model. The BoB 23 November $CDF(\varepsilon)$ distribution, however, strongly deviates from the best possible lognormal approximation, showing at the same time the lowest median value of $\varepsilon \approx 7.7 \times 10^{-10}$ W/kg. This number is about ten or even hundred times smaller than the other medians shown in the same figure. It may imply that the ML $CDF(\varepsilon)$ of 23 November describes dissipation data taken from a buried mixed layer ($15 < z < 45$) where wind-induced turbulence and active mixing almost ceased, being suppressed by a sharp diurnal pycnocline. It is also possible that the generation and dissipation of upper layer turbulence in the presence of multiple frontal zones could be a unique feature of the northern BoB, which requires better understanding of the process and much more extensive data for statistical analysis.

The examples of $CDF(\varepsilon)$ given in Figure 9 (as well as the GS_S ML $CDF(\varepsilon)$, which is not shown in the plot as it almost coincides with the 21 November CDF) indicate that the probability distribution of dissipation rate in turbulent, actively mixing layers can be approximated by lognormal model, which is in agreement with Gurvich and Yaglom (1967) and previous observations in surface layers of oceans and lakes (e.g., Lozovatsky et al., 2006; Planella et al., 2011; Thorpe et al., 2008). At the same time, the Burr distribution could be as good as lognormal model in application to ML $CDF(\varepsilon)$, with Burr model having some advantage. Thus Burr model is a suitable competitor for approximating $CDF(\varepsilon)$ for active (mixing layer) as well as decaying (mixed layer) turbulence.
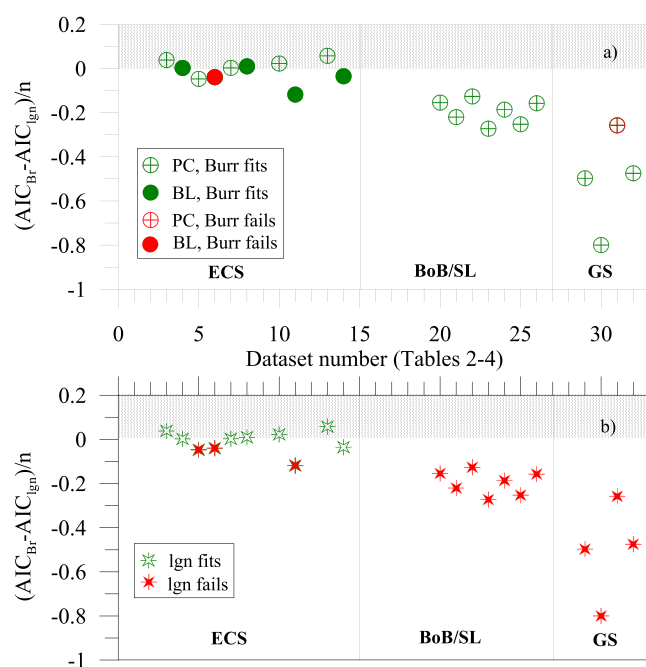

Figure 8. The normalized difference between Akaike information criteria calculated for the Burr AIC_{Br} and lognormal $AIC_{\lg n}$ models fitted to the empirical probability distributions of ε shown in Figures 4–7 and numbered in Tables 2–4. A negative $\left(AIC_{Br} - AIC_{\lg n}\right)/n$ favors the Burr approximation over the lognormal one and vice versa; (a) results of the Kolmogorov-Smirnov test for the Burr model for each data set; (b) results of the same test for the lognormal model. Green symbols indicate CDFs, for which the tested approximation cannot be rejected, otherwise the red symbols (the model does not fit the data with 0.05 significance level). PC, pycnocline; BL, boundary layer.
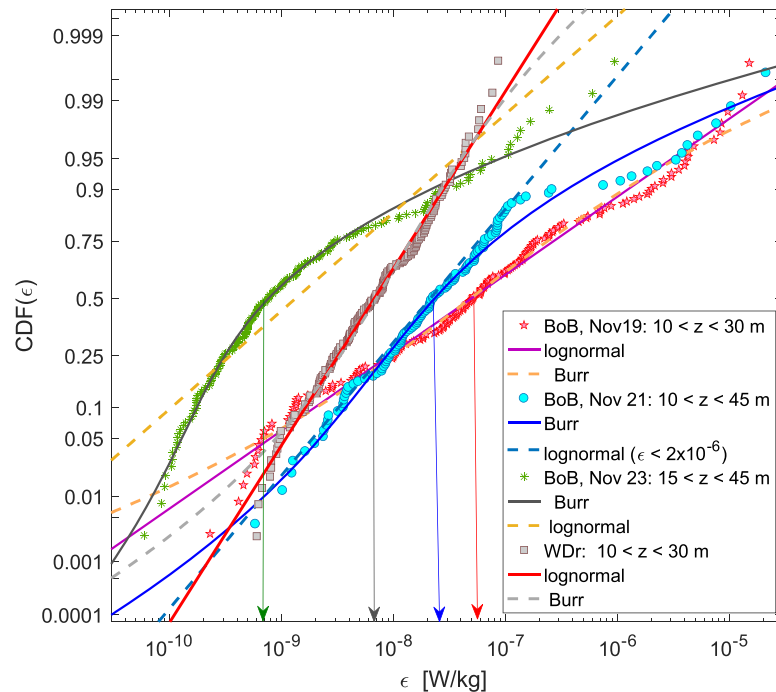
Figure 9. The cumulative distribution functions $CDF(\varepsilon)$ for the dissipation rate ε_{ml} in the surface mixed layer (ML, the depth range is in the legend) in the BoB (19–23 November stations) and along the Weligama drift (WDr). Parameters for Burr and lognormal distributions are in Table 5. The medians are shown by arrows. The less favorable approximation among the two is dashed.

3.3. Interplay Between Parameters of the Burr Approximation

The Burr distribution, which approximates most of the dissipation records analyzed in this study, is a three parameters distribution (so is the generalized extreme value distribution [Lozovatsky, Lee, et al., 2015]), which could be considered as a disadvantage compared to competing distributions such as lognormal or sometimes Weibull that are specified by two parameters. We, however, found that two independent shape parameters of the Burr distribution $c_{Br} \equiv c$ and $k_{Br} \equiv k$ (equations (3) and (4)) are interrelated when the model is applied to the dissipation rate CDFs. Figure 10 shows the regression plot of $\log_{10} k_{Br}$ versus $\log_{10} c_{Br}$, indicating an inverse dependence $c_{Br} = 1.26/k_{Br}$ with the coefficient of determination $r^2 = 0.8$. As such, the Burr distribution (4) for ε can be rewritten as

$$CDF_B(\varepsilon) = 1 - \left(1 + (\varepsilon_0/\varepsilon)^{bk}\right)^{-k}, \qquad (4a)$$

with only one shape parameter $k > 0$, a scale parameter ε_0, and a constant b, which is about 0.8 (close to unity). Equation (4a) represents the inverse Burr or the Dagum distribution (Dagum, 1977) wherein the shape parameters of the Burr are functionally related. An increasing trend of the shape parameter k_{Br} (k) with the increase of the scale parameter ε_0 (which can be interpreted as a characteristic dissipation rate in the region) is shown in Figure 11, however the GS pycnocline data are not in line with this notion. Formally, k_{Br} and ε_0 could be completely independent, but it is possible that the probability distribution of dissipation rate in ocean may have a tendency to be more skewed (larger values of the shape parameter) for more active turbulence (larger ε_0). This preliminary finding requires more scrutiny based on more extensive data sets.

3.3.1. Skewness and Kurtosis of the Dissipation Rate in the Ocean

The skewness of the dissipation rate (Sk_ε) as well as its kurtosis (K_ε) are important parameters that indicate the degree of intermittency of oceanic turbulence. To our knowledge, however, the *relationship* between Sk_ε and K_ε for oceanic
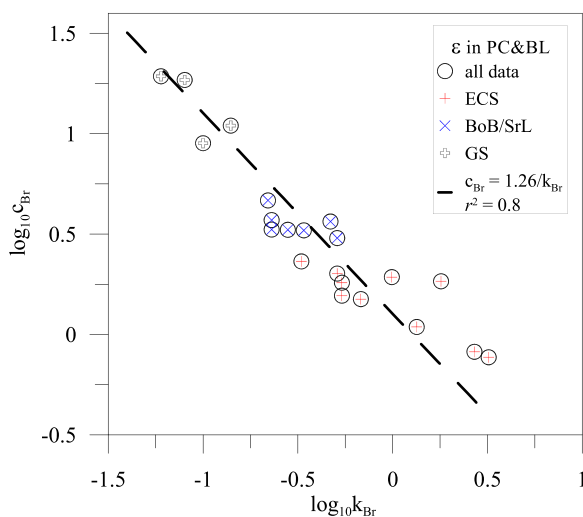

Figure 10. An inverse power approximation of the correlation between Burr shape parameters $c_{Br} \equiv c$ and $k_{Br} \equiv k$ (equation (3)) for ECS, BoB/SL, and GS pycnoclines (PC) and the ECS bottom layer (BL).
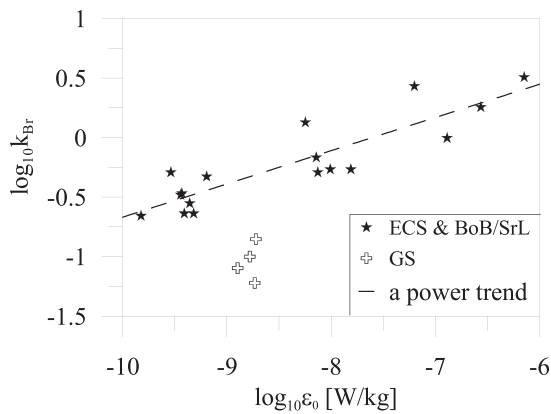
Figure 11. The shape parameter k_{Br} of the Burr approximations of $CDF(\varepsilon)$ versus its scale parameter ε_0 for ECS, BoB/SL, and GS pycnoclines and ECS bottom layer.

turbulence has not been analyzed yet. Soloviev (1990) was among the first to calculate the skewness $Sk_{dT/dt}$ of small-scale temperature derivatives dT/dt in oceanic surface layer, finding it to be negative (between -0.7 and -1.0) during nighttime convection but positive during day-time stable stratification. Thorpe et al. (1991) obtained similar results for $Sk_{dT/dt}$ in a boundary layer above a sloping bottom. Thorpe and Osborn (2005) and Thorpe et al. (2008) further examined $Sk_{dT/dt}$ across a mixed water column on a tidal shelf as well as the skewness of the gradient $d(\log \varepsilon)/dt$. They also found that $Sk_{\log \varepsilon}$ itself was mostly close to zero (the kurtosis of $\log \varepsilon$ was about 3), in agreement with often observed normal distribution of $\log \varepsilon$ in nonstratified turbulent layers. The skewness of the gradient $Sk_{d(\log \varepsilon)/dt}$, however, appeared to be nonzero, though small. The authors attributed the observed correspondence between the signs of $Sk_{dT/dt}$ and $Sk_{d(\log \varepsilon)/dt}$ to possible advection of small-scale turbulence by billows in a tidal shear flow.

As mentioned, the *relationship* between skewness and kurtosis of dissipation rate, which is proportional to the variance $\overline{(\partial u'_i/\partial x_i)^2}$ (here $i = 1$–3), has not been examined yet, although a number of publications have dealt with Sk and K of a derivative $\partial u'_i/\partial x_i$ (e.g., Kholmyansky et al., 2001; Sreenivasan & Antonia, 1997; Van Atta & Antonia, 1980). For example, various laboratory and atmospheric data examined by Van Atta and Antonia (1980) showed that at the scales on the order of the Taylor microscale λ, both Sk and K of $\partial u'_i/\partial x_i$ are dependent on the turbulent Reynolds number $R_\lambda = rms(u'_i)\lambda/v$ according to the empirical relation $-Sk = 0.23K^{0.362}$, which is close to their own (as well as Wyngaard & Tennekes' (1970)) modeling prediction $Sk \sim K^{3/8}$.

Skewness and kurtosis for any probability distribution are not independent but follow $K \geq Sk^2 + 1$ (e.g., Krishnamoorthy, 2006), that is the full kurtosis can never be less than 1 and the excess kurtosis $(K-3)$ cannot drop below -2. For atmospheric turbulence, the correspondence between Sk and K of both scalar and wind velocity fluctuations has been reported by Mole and Clarke (1995), Alberghi et al., (2002), and Maurizi (2006). These authors attempted a generalized relationship, namely $K = a(Sk^2 + 1)$ based on the above mentioned statistical limit $K \geq (Sk^2 + 1)$ (Kendall & Stuart, 1977). Maurizi (2006) speculated that for vertical velocity fluctuations in stably stratified layers, the coefficient a could be an increasing function of the gradient Richardson number, however, no convincing evidence was offered.

A regression plot of K_ε versus Sk_ε, which employs all our dissipation rate data for ECS, BoB/SL, and GS, is shown in Figure 12 (28 points in total). The data samples follow the expected theoretical dependence

$$K_\varepsilon = a\left(Sk_\varepsilon^2 + 1\right) \tag{9a}$$

over a wide range of Sk_ε and K_ε. The constant $a = 1.26 \pm 0.01$ (the least absolute residuals estimate). Note also that the entire data set can be approximated by an empirical expansion of (9a)

$$K_\varepsilon = a_1 Sk_\varepsilon^2 + b, \tag{9b}$$

where a_1 and b are some constants (Shaw & Seginer, 1987; Schopflocher & Sullivan, 2005). In our case, $a_1 = 1.25$ and $b = 2.95$ define the curve in Figure 12, which is almost indistinguishable from that of (9a). Because a majority of the data (17 out of 28 points) are concentrated at relatively low values of skewness and kurtosis, an enlarged plot of $K_\varepsilon(Sk_\varepsilon)$ for $Sk_\varepsilon < 10$ is shown in the insert of Figure 12; formula (9a) fits this subset of data very well with a slightly larger value of $a = 1.31$.
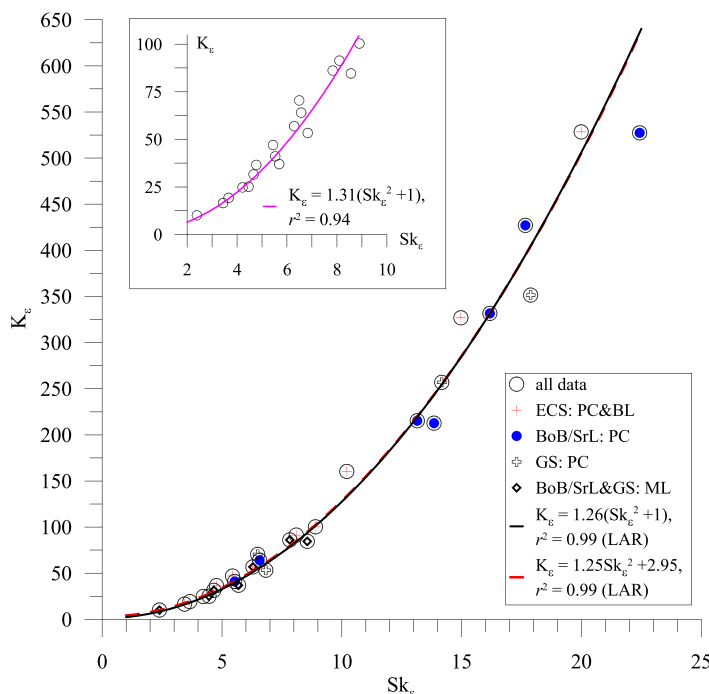

Figure 12. The kurtosis K_ε as a function of skewness Sk_ε of the dissipation rate measured in the BoB/SL and GS pycnocline and mixed layer (PC, ML) as well as in the PC and bottom layers (BL) of the ECS. Data for $Sk_\varepsilon < 10$ are in insert. The quadratic approximations are in the legends (LAR is the least absolute residuals method used in MATLAB curve fitting application).

Thus, we conclude that a one-parameter quadratic model (9a) nicely approximates the relationship between the dissipation rate skewness and kurtosis for the data sets of this study. Our analysis of Sk_ε and K_ε of oceanic turbulence, however, does not indicate any dependence of the parameter a (9a) on flow stability (Richardson number) as has been suggested by Maurizi (2006) for wind velocity fluctuations.

4. Conclusions

Our analysis of the dissipation rate records collected in deep (the northern Indian Ocean and the Gulf Stream region) and shallow waters (the East China Sea) with characteristic equidistant vertical averaging of individual samples ∼1.4 m suggests that the Burr type XII probability distribution is an appropriate statistical model for the distribution of ε in *ocean pycnocline*, whereas lognormal model does not perform as good. In weakly stratified boundary layers, however, both statistical models compete equally well with lognormal model performing somewhat better.

It was also found that the two shape parameters of the Burr distribution (4) are functionally related, with $c_{Br} = 1.26/k_{Br}$, thus reducing the three-parameter Burr distribution to a two-parameter distribution (4a), which is also called the Dagum distribution. This is an indication that the distribution of ε in the ocean pycnocline may be more skewed (larger values of the Burr shape parameter) toward more energetic turbulence events (larger values of the dissipation rate). This latter postulation requires further corroboration with more extensive data sets.

Because skewness and kurtosis of turbulent fluctuations are important characteristics of turbulence intermittency in environmental flows, we, for the first time, examined the relationship between Sk_ε and K_ε for oceanic turbulence. The values of Sk_ε and K_ε calculated for all 28 available records of ε varied from 1 to 100 for Sk_ε and from 3 to 700 for K_ε, and exhibited remarkably strong one-parameter quadratic dependence between Sk_ε and K_ε (9a), which approximated well the data obtained in sharp pycnoclines, weakly stratified bottom layers or in almost homogeneous surface mixed layers.

From the probabilistic point of view, the generation/dissipation of energetic turbulence in strongly stratified pycnoclines, like those in the summertime ECS, in the northern BoB and all the way around Sri Lanka, can be considered as a random sequence of rare events. The sources of turbulence therein are most probably associated with nonstationary, intermittent internal-wave breaking (e.g., Gregg et al., 1993; Moum & Rippeth, 2009) and sporadic shear-induced instabilities (e.g., Strang & Fernando, 2001; Thorpe et al., 2008). In less stratified layers and in regions with sustainable shear instability (like, for example, Equatorial undercurrents), the mesoscale intermittency of dissipation rate could be specified by more traditional lognormal distribution (e.g., Baker & Gibson, 1987; Jinadasa et al., 2013; Wijesekera et al., 1993). Even for such layers, however, the Burr distribution is a good model to represent stochastic nature of oceanic turbulence.

The dependence of parameters pertinent to ε distributions on statistical quantities that describe background flow such as buoyancy frequency, vertical shear, and the gradient Richardson number (e.g., Gregg et al., 1993; Lozovatsky & Erofeev, 1993) is of considerable practical interest, and should be addressed in future studies.

References

Akaike, H. (1974). A new look at the statistical model identification. *IEEE Transactions on Automatic Control*, 19(6), 716–723.
Alberghi, S., Maurizi, A., & Tampieri, F. (2002). Relationship between the vertical velocity skewness and kurtosis observed during seabreeze convection. *Journal of Applied Meteorology*, 41, 885–889.
Baker, M. A., & Gibson, C. H. (1987). Sampling turbulence in the stratified ocean: Statistical consequences of strong intermittency. *Journal of Physical Oceanography*, 17, 1817–1837. https://doi.org/10.1175/1520-0485(1987)017<1817:STITSO>2.0.CO;2
Baumert, H. Z., Simpson, J. H., & Sündermann, J. (Eds.). (2005). *Marine turbulence: Theories, observations and models* (652. pp.). Cambridge, UK: Cambridge University Press.
Bozdogan, H. (1987). Model selection and Akaike's information criterion (AIC): The general theory and its analytical extensions. *Psychometrika*, 52, 345–370.
Burr, I. W. (1942). Cumulative frequency functions. *Annals of Mathematical Statistics*, 13, 215–232.
Cuypers, Y., Bouruet-Aubertot, P., Marec, C., & Fuda, J. L. (2012). Characterization of turbulence from a fine-scale parameterization and microstructure measurements in the Mediterranean Sea during the BOUM experiment. *Biogeosciences*, 9(8), 3131–3149.
Dagum, C. (1977). A new model of personal income distribution: Specification and estimation, *Economie Appliquee*, 30, 413–437.
Frisch, U. (1995). *Turbulence: The legacy of A.N. Kolmogorov* (296 pp.). Cambridge, UK: Cambridge University Press.
Gregg, M. C. (1999). Uncertainties and limitations in measuring ε and χ. *Journal of Atmospheric and Oceanic Technology*, 16, 1483–1490.
Gregg, M. C., Seim, H. E., & Percival, D. B. (1993). Statistics of shear and turbulent dissipation profiles in random internal wave fields. *Journal of Physical Oceanography*, 23, 1777–1799.

Gregg, M. C., Winkel, D. P., Sanford, T. B., & Peters, H. (1996). Turbulence produced by internal waves in the oceanic thermocline at mid and low latitudes. *Dynamics of Atmospheres and Oceans*, *24*, 1–14.

Gurvich, A. S., & Yaglom, A. M. (1967). Breakdown of eddies and probability distributions for small scale turbulence. *Physics of Fluids*, *10*, 54–65.

Hebert, D., Moum, J. N., Paulson, C. A., & Caldwell, D. R. (1992). Turbulence and internal waves at the equator. Part II: Details of a single event. *Journal of Physical Oceanography*, *22*, 1346–1356.

Jinadasa, S. U. P., Lozovatsky, I. D., & Fernando, H. J. S. (2013). Small-scale and lateral intermittency of oceanic microstructure in the pycno-cline. *Physica Scripta*, *T155*, 014035. https://doi.org/10.1088/0031-8949/2013/T155/014035

Jinadasa, S. U. P., Lozovatsky, I., Planella-Morató, J., Nash, J. D., MacKinnon, J. A., Lucas, A. J., . . . Fernando, H. J. S. (2016). Ocean turbulence and mixing around Sri Lanka and in adjacent waters of the northern Bay of Bengal. *Oceanography*, *29*(2), 170–179. https://doi.org/10.5670/oceanog.2016.49

Kendall, M. G., & Stuart, A. (1977). *The advanced theory of statistics* (Vol. 1, 168 pp.). New York: Macmillan.

Kholmyansky, M., Tsinober, A., & Yorish, S. (2001). Velocity derivatives in the atmospheric surface layer at $Re_\lambda = 104$. *Physics of Fluids*, *13*, 311–314.

Kolmogorov, A. N. (1962). A refinement of previous hypotheses concerning the local structure of turbulence in a viscous incompressible fluid at high Reynolds number. *Journal of Fluid Mechanics*, *13*, 82–85. https://doi.org/10.1017/S0022112062000518

Kotz, S., & Nadarajah, S. (2000). *Extreme value distributions: Theory and applications* (185 pp.). London, UK: Imperial College Press.

Krishnamoorthy, K. (2006). *Handbook of statistical distributions with applications [Statistic: A Series of Textbook and Monographs]* (376 pp.). Boca Raton, FL: Chapman and Hall.

Kuo, A. Y. C., & Corrsin, S. (1971). Experiments on internal intermittency and fine-structure distribution functions in fully turbulent fluid. *Journal of Fluid Mechanics*, *50*(2), 285–319. https://doi.org/10.1017/S0022112071002581

Lie, H.-J., & Cho, C.-H. (2016). Seasonal circulation patterns of the Yellow and East China Seas derived from satellite-tracked drifter trajecto-ries and hydrographic observations. *Progress in Oceanography*, *146*, 121–141. https://doi.org/10.1016/j.pocean.2016.06.004

Liu, Z., Wei, H., Lozovatsky, I. D., & Fernando, H. J. S. (2009). Late summer stratification, internal waves and turbulence in the Yellow Sea. *Journal of Marine Systems*, *77*, 459–472. https://doi.org/10.1016/j.jmarsys.2008.11.001

Lozovatsky, I., Jinadasa, S. U. P., Fernando, H. J. S., Lee, J.-H., & Hong, C.-S. (2015). The wall-layer dynamics in a weakly stratified tidal bottom boundary layer. *Journal of Marine Research*, *73*, 207–232.

Lozovatsky, I., Lee, J.-H., Fernando, H. J. S., Kang, S. K., & Jinadasa, S. U. P. (2015). Turbulence in the East China Sea: The summertime stratifi-cation. *Journal of Geophysical Research: Oceans*, *120*, 1856–1871. https://doi.org/10.1002/2014JC010596

Lozovatsky, I., Liu, Z., Fernando, H. J. S., Armengol, J., & Roget, E. (2012). Shallow water tidal currents in close proximity to the seafloor and boundary-induced turbulence. *Ocean Dynamics*, *62*, 177–201. https://doi.org/10.1007/s10236-011-0495-3

Lozovatsky, I., Planella-Morato, J., Sherman, K., Wang, Q., & Fernando, H. J. S. (2017). Vertical mixing and elements of mesoscale dynamics over North Carolina shelf and contiguous Gulf Stream waters. *Ocean Dynamics*, *67*, 783–798. https://doi.org/10.1007/s10236-017-1059-y

Lozovatsky, I., Roget, E., Figueroa, M., Fernando, H. J. S., & Shapovalov, S. (2006). Sheared turbulence in weakly stratified upper ocean. *Deep Sea Research Part I: Oceanographic Research Papers*, *53*, 387–407.

Lozovatsky, I., Roget, E., Planella, J., Fernando, H. J. S., & Liu, Z. (2010). Intermittency of near-bottom turbulence in tidal flow on a shallow shelf. *Journal of Geophysical Research*, *115*, C05006. https://doi.org/10.1029/2009JC005325

Lozovatsky, I. D., & Erofeev, A. Y. (1993). Statistical approach to eddy viscosity simulation for numerical models of the upper turbulent oce-anic layer. *Journal of Marine Systems*, *4*, 391–399.

Mandelbrot, B. B. (1974). Intermittent turbulence in self-similar cascades: Divergence of high moments and dimension of the carrier. *Jour-nal of Fluid Mechanics*, *62*, 331–358.

Massey, F. J. (1951). The Kolmogorov-Smirnov test for goodness of fit. *Journal of the American Statistical Association*, *46*(253), 68–78.

Maurizi, A. (2006). On the dependence of third- and fourth-order moments on stability in the turbulent boundary layer. *Nonlinear Processes in Geophysics*, *13*, 119–123.

Mole, N., & Clarke, E. D. (1995). Relationships between higher moments of concentration and of dose in turbulent dispersion. *Boundary-Layer Meteorology*, *73*, 35–52.

Monin, A. S., & Yaglom, A. M. (1975). *Statistical fluid mechanics: Mechanics of turbulence* (Vol. 2, 874 pp.). Cambridge, MA: MIT Press.

Moum, J. N., Caldwell, D. R., & Paulson, C. A. (1989). Mixing in the equatorial surface layer and thermocline. *Journal of Geophysical Research*, *94*, 2005–2021.

Moum, J. N., & Rippeth, T. P. (2009). Do observations adequately resolve the natural variability of oceanic turbulence? *Journal of Marine Sys-tems*, *77*, 409–417. https://doi.org/10.1016/j.jmarsys.2008.10.013

Novikov, E. A. (1970). Intermittency and scale similarity in the structure of a turbulent flow. *Journal of Applied Mathematics and Mechanics*, *35*, 266–277.

Obukhov, A. M. (1962). Some specific features of atmospheric turbulence. *Journal of Fluid Mechanics*, *13*, 77–81. https://doi.org/10.1017/S0022112062000506

Okasha, M. K., & Matter, M. Y. (2015). On the three-parameter Burr type XII distribution and its application to heavy tailed lifetime data. *Journal of Advances in Mathematics*, *10*(4), 3529–3442.

Peters, H., Gregg, M. C., & Sanford, T. B. (1995). Detail and scaling of turbulent overturns in the Pacific Equatorial Undercurrent. *Journal of Geophysical Research*, *100*, 18,349-18,368.

Planella, J., Roget, E., & Lozovatsky, I. (2011). Statistics of microstructure patchiness in a stratified lake. *Journal of Geophysical Research*, *116*, C10035. https://doi.org/10.1029/2010JC006911

Prandke, H., & Stips, A. (1998). Test measurements with an operational microstructure-turbulence profiler: Detection limits of dissipation rates. *Aquatic Sciences*, *60*, 191–209.

Rachev, S. T., Hoechstetter, M., Fabozzi, F. J., & Focardi, S. M. (2010). *Probability and statistics in finance* (672 pp.). Hoboken, NJ: John Wiley and Sons.

Rodriguez, N. (1977). A guide to the Burr type XII distributions. *Biometrika*, *64*, 129–134.

Roget, E., Lozovatsky, I., Sanchez, X., & Figueroa, M. (2006). Microstructure measurements in natural waters: Methodology and applications. *Progress in Oceanography*, *70*, 123–148.

Rousseau, S., Kunze, E., Dewey, R., Bartlett, K., & Dower, J. (2010). On turbulence production by swimming marine organisms in the open ocean and coastal waters. *Journal of Physical Oceanography*, *40*(9), 2107–2121.

Schopflocher, T. R., & Sullivan, P. J. (2005). The relationship between skewness and kurtosis of a diffusing scalar. *Boundary-Layer Meteorol-ogy*, *115*, 341–358.

Seuront, L. (2008). Microscale complexity in the ocean: Turbulence, intermittency and plankton life. *Mathematical Modelling of Natural Phenomena*, *3*(3), 1–41.

Seuront, L., Yamazaki, H., & Schmitt, F. G. (2005). Intermittency. In H. Baumert, J. Sundermann, & J. Simpson (Eds.), *Marine turbulence: Theories, observations and models* (pp. 66–78). Cambridge, UK: Cambridge University Press.

Shaw, R. H., & Seginer, I. (1987). Calculation of velocity skewness in real and artificial plant canopies. *Boundary-Layer Meteorology*, *39*(3), 15–332.

Soloviev, A. V. (1990). Coherent structure at the ocean surface in convectively unstable conditions. *Nature*, *346*, 157–160.

Sreenivasan, K. R., & Antonia, R. A. (1997). The phenomenology of small-scale turbulence. *Annual Review of Fluid Mechanics*, *29*, 435–472. https://doi.org/10.1146/annurev.fluid.29.1.435

Strang, E. J., & Fernando, H. J. S. (2001). Vertical mixing and transports through a stratified shear layer. *Journal of Physical Oceanography*, *31*(8), 2026–2048.

Tadikamalla, P. R. (1980). A look at the Burr and related distributions. *International Statistical Review*, *48*, 337–344.

Tennekes, H., & Lumley, J. L. (1972). *A first course in turbulence* (300 pp.). Cambridge, MA: The MIT Press.

Thorpe, S. A., Curé, M., & White, M. (1991). The skewness of temperature derivatives in oceanic boundary layers. *Journal of Physical Oceanography*, *21*, 428–433.

Thorpe, S. A., Green, J. M., Simpson, J. H., Osborn, T. R., & Smith, W. (2008). Boils and turbulence in a weakly stratified shallow tidal sea. *Journal of Physical Oceanography*, *38*, 1711–1730. https://doi.org/10.1175/2008JPO3931.1

Thorpe, S. A., & Osborn, T. R. (2005). Skewness of spatial gradients of turbulent dissipation rates in the mixed layer. *Journal of Physical Oceanography*, *35*, 2299–2303.

Tsinober, A. (2001). *An informal introduction to turbulence* (324 pp.). Dordrecht, The Netherlands: Kluwer.

Van Atta, C. W., & Antonia, R. A. (1980). Reynolds number dependence of skewness and flatness factors of turbulent velocity derivatives. *Physics of Fluids*, *23*(2), 252–257.

Wijesekera, H. W., Dillon, T. M., & Padman, L. (1993). Some statistical and dynamical properties of turbulence in the oceanic pycnocline. *Journal of Geophysical Research*, *98*, 665–679.

Wijesekera, H. W., Shroyer, E. L., Tandon, A., Ravichandran, M., Sengupta, D., Jinadasa, S. U. P., . . . Whalen, C. B. (2016). ASIRI: An ocean-atmosphere initiative for Bay Bengal. *Bulletin of the American Meteorological Society*, *97*, 1859–1884.

Wolk, F., Yamazaki, H., Seuront, L., & Lueck, R. G. (2002). A new free-fall profiler for measuring biophysical microstructure. *Journal of Atmospheric and Oceanic Technology*, *19*(5), 780–793.

Wyngaard, J. C., & Tennekes, H. (1970). Measurements of the small-scale structure of turbulence at moderate Reynolds numbers. *Physics of Fluids*, *13*(2), 1962–1969.

Yamazaki, H. (1990). Breakage models: Lognormality and intermittency. *Journal of Fluid Mechanics*, *219*, 181–193.

Yamazaki, H., & Lueck, R. G. (1990). Why oceanic dissipation rates are not lognormal, *Journal of Geophysical Research: Oceans*, *20*, 1907–1918.

Zhang, J., Huang, D., Xiao, T., Liu, S., & Fang, J. (2016). Response of biogeochemical cycles and ecosystem in the East China Sea to multistressors. *Deep Sea Research Part II: Topical Studies in Oceanography*, *124*, 1–5.

Zimmer, W. J., Keats, J. B., & Wang, F. K. (1998). The Burr XII distribution in reliability analysis. *Journal of Quality Technology*, *30*(4), 386–394.